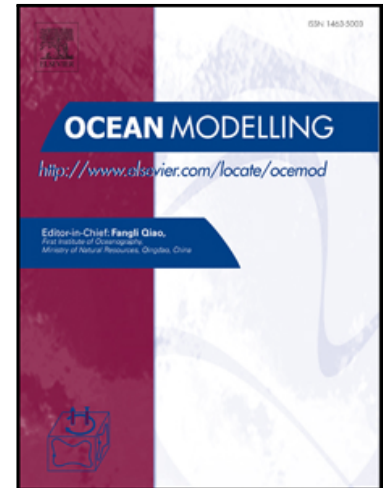# Journal Pre-proof

Disentangling Wavy and Vortical Motions in Concurrent Snapshots of the Sea Surface Height and Velocity

Chuanyin Wang , Zhiyu Liu , Hongyang Lin , Cesar Rocha ,
Qinghua Yang , Dake Chen , Junbin Gong

Please cite this article as: Chuanyin Wang , Zhiyu Liu , Hongyang Lin , Cesar Rocha , Qinghua Yang , Dake Chen , Junbin Gong , Disentangling Wavy and Vortical Motions in Concurrent Snapshots of the Sea Surface Height and Velocity, *Ocean Modelling* (2025), doi: https://doi.org/10.1016/j.ocemod.2025.102556

Highlights:

- The challenge of separating vortical and wavy motions is tackled
- The separation uses the fact that wavy motions bear no potential vorticity anomaly
- The separation applies to a concurrent snapshot of sea surface height and velocity
- The separation is simple and efficient, with a numerical simulation as a testbed

Disentangling Wavy and Vortical Motions in Concurrent Snapshots of the Sea Surface Height and Velocity

Chuanyin Wang[a], Zhiyu Liu[b], Hongyang Lin[b], Cesar Rocha[c], Qinghua Yang[a], Dake Chen[a,d], and Junbin Gong[e]

[a]School of Atmospheric Sciences, Sun Yat-sen University, and Southern Marine Science and Engineering Guangdong Laboratory (Zhuhai), Zhuhai, China

[b]State Key Laboratory of Marine Environmental Science, and Department of Physical Oceanography, College of Ocean and Earth Sciences, Xiamen University, Xiamen, China

[c]Universidade de São Paulo, São Paulo, Brazil

[d]State Key Laboratory of Satellite Ocean Environment Dynamics, Second Institute of Oceanography, Ministry of Natural Resources, Hangzhou, China

[e]Hanjiang National Laboratory, Wuhan, China

Correspondence to: Zhiyu Liu, zyliu@xmu.edu.cn

2

Abstract

Wide-swath satellite missions, such as Surface Water and Ocean Topography (SWOT) and Ocean Dynamics and Sea Exchanges with the Atmosphere (ODYSEA), will provide quasi-concurrent observations of the two-dimensional sea surface height and velocity. Thanks to their high spatial resolution, the spatial features of both vortical and wavy oceanic motions are expected to be captured by these observations. A natural question is whether one can disentangle vortical and wavy motions in these snapshot observations. This issue has attracted some efforts, but crucial progress remains to be made. Here, assuming that only a single concurrent snapshot of the sea surface height and velocity is available, we pursue a dynamical approach for disentangling vortical and wavy motions. This is realized by noting that wavy motions do not induce potential vorticity anomalies. A proof-of-concept application using an output of a realistic high-resolution numerical simulation suggests that the proposed approach is simple and efficient, and is particularly useful for separating wavy and vortical motions in observations by wide-swath satellite missions.

1. Introduction

There exist two fundamental types of oceanic motions, namely vortical and wavy motions. Large-scale currents, mesoscale flows and submesoscale processes are typical examples of vortical motions, which generally transport tracers along the isopycnal. An enduring topic in coarse-resolution ocean models is the parameterization of the isopycnal mixing induced by mesoscale flows (Gent and Mcwilliams, 1990; Griffies, 1998). Barotropic tides and internal gravity waves (IGWs) are representative of wavy motions, which through generation of small-scale turbulence significantly contribute to the diapycnal mixing. A challenging topic is to faithfully constrain the diapycnal mixing resulting from IGWs (Gregg, 2021; Jayne, 2009; St. Laurent et al., 2002). Due to their contrasting implications for ocean mixing, it is essential to disentangle vortical and wavy motions and to deepen the understanding of their respective characteristics.

Our understanding of both vortical and tidal motions has largely hinged on nadir-looking satellite altimeters (e.g., Morrow et al., 2023), which measure a one-dimensional section of the sea surface height (SSH) with an along-track resolution of 6-7 km (e.g., Fu and Ubelmann, 2014), a cross-track spacing of 200-300 km (e.g., Fu and Ubelmann, 2014) and a repeat period of 10 days (e.g., Le Traon, 2013). Over the last ~30 years, large-scale and mesoscale signals have been extracted from the measured SSH to study the variability of ocean currents, changes

of the mean sea level (Fu and Chelton, 2001), as well as the dynamics of mesoscale vortices and eddy-mean flow interactions (Le Traon and Morrow, 2001). At the same time, global barotropic tides have been estimated with the observed SSH through data assimilation (Provost, 2001), and are suggested to provide about half of the mechanical energy required to maintain the global overturning circulation (Egbert and Ray, 2000, 2001, 2003); moreover, low-mode coherent baroclinic tidal SSH has been separated from satellite altimeter data according to aliasing principles of tides (Carrère et al., 2004; Dushaw, 2015; Kantha and Tierney, 1997; Ray and Zaron, 2016; Ray and Cartwright, 2001; Ray and Mitchum, 1996; Zaron, 2019; Zhao, 2017; Zhao et al., 2016), and the energetics of baroclinic tides have been quantified (Kantha and Tierney, 1997; Ray and Cartwright, 2001; Zaron et al., 2022; Zhao, 2017; Zhao et al., 2016). Therefore, nadir-looking satellite altimetry has been widely recognized as an oceanographic revolution (Abdalla et al., 2021; Morrow et al., 2023; Le Traon, 2013).

In spite of its revolutionary success, the conventional altimetry is incapable of resolving submesoscale flows and the internal gravity wave continuum due to its nadir-looking nature. This has motivated the development of wide-swath satellite altimetry, including the Surface Water and Ocean Topography (SWOT; Fu and Ubelmann, 2014; Morrow et al., 2019; Fu et al., 2024) and Guanlan (Chen et al., 2019) missions. By design, the wide-swath satellite altimetry can effectively observe the ocean by taking a two-dimensional snapshot of SSH (Morrow et al., 2019) with a swath width of ~50 km, a horizontal resolution of ~2 km and a repeat period of ~20 days (Fu et al., 2024). Also being planned is the wide-swath Doppler scatterometry, such as the Ocean Dynamics and Sea Exchanges with the Atmosphere (ODYSEA) and the Ocean Surface Current multiscale Observation Mission (OSCOM), which is designed to measure sea surface velocity (SSV) with a swath width of ~1000 km, a horizontal resolution of ~5 km and a global coverage of ~1 day (Bourassa et al., 2016; Du et al., 2021; Rodríguez et al., 2019; Torres et al., 2023). Wide-swath satellite altimetry and scatterometry will be useful in observing larger submesoscale flows and longer IGWs. It is thus expected that new perspectives on vortical and wavy dynamics will be revealed (Du et al., 2021; Morrow et al., 2019). However, these wide-swath observations will remain with a low temporal resolution due to the long revisit period of satellites, and thus the temporal evolution of oceanic flows will be undersampled; as such, disentangling vortical and wavy motions with methods based on full spatio-temporal information, such as the dynamical decomposition devised by C. Wang et al. (2023a), is not possible. Hence, a major challenge in the application of these unprecedented

data is to disentangle vortical and wavy motions captured by the two-dimensional snapshots of SSH and SSV (Morrow et al., 2019).

Several attempts have been made to address this problem. In an idealized model configuration where an unstable baroclinic jet is subject to mode-1 baroclinic tidal forcing, Ponte et al. (2017) used a two-dimensional snapshot of sea surface density to estimate three-dimensional potential vorticity through an empirical formula, then inverted quasi-geostrophic potential vorticity to obtain the geostrophic SSH, and finally obtained the tidal SSH as the difference between the total and geostrophic SSH. With the ground truth from the same numerical simulation as Ponte et al. (2017), Le Guillou et al. (2021) presented an alternating minimization approach that iteratively assimilates two-dimensional SSH into a 1.5-layer quasi-geostrophic model to map vortical SSH and a 1.5-layer linear shallow water model to get baroclinic tidal SSH. Using outputs of a realistic, tide-resolving and submesoscale-admitting numerical simulation, Torres et al. (2019) spatially low-pass (high-pass) filtered snapshots of SSH to extract vortical (wavy) components with the cutoff wavelength chosen to be the scale where the summertime SSH wavenumber spectra displayed a significant slope discontinuity. In idealized and realistic model configurations, recent machine-learning techniques have also proved useful in extracting signal of baroclinic tides from SSH snapshots (Lguensat et al., 2020; H. Wang et al., 2022).

In summary, existing approaches are mainly based on SSH, and mostly work only for specific settings. By contrast, this study, using both SSH and SSV in anticipation of wide-swath satellite missions, formulates the problem of vortical-wavy disentanglement as a general initialization problem. Specifically, we consider the scenario where only a single pair of concurrent snapshots of SSH and SSV is available, and invokes the property that wavy motions do not induce any potential vorticity anomaly to decompose the full flow into vortical and wavy components. The paper is structured as follows. The proposed decomposition approach is presented in Section 2. Proof-of-concept applications of the proposed approach to simulated flows from a realistic, tide-resolving and submesoscale-admitting simulation are shown in Section 3. The results are summarized and discussed in Section 4.

2. Methodology

2.1 Mathematical formulation

The defining feature of wavy motions is that the polarization relation relating wavy pressure and velocity and the dispersion relation relating wavy frequencies and wavenumbers are satisfied. An immediate corollary is the well-recognized property that wavy motions bear no potential vorticity anomaly (Pedlosky, 2003; Zeitlin, 2018).[1] This basic property has been directly used as a definition of wavy motions no matter the system is linear or nonlinear (e.g., Viúdez and Dritschel, 2004; Dritschel and Viúdez, 2007). In the history of numerical weather prediction, this property has spawned an ingenious idea of addressing an initialization problem that intends to eliminate IGWs from initial fields in order to accurately predict meteorologically-important phenomena that are generally in geostrophic balance (e.g., Zeitlin, 2018). Assuming that only a snapshot of SSH and SSV is given, this idea can be formulated in the quasi-geostrophic regime as follows:

$$\nabla^2 \left(\frac{g\bar{\eta}}{f_0}\right) - \frac{1}{L_d^2}\frac{g\bar{\eta}}{f_0} = \Pi = \zeta - \frac{1}{L_d^2}\frac{g\eta}{f_0}, \tag{1a}$$

$$\boldsymbol{f_0} \times \bar{\boldsymbol{u}} = -g\nabla\bar{\eta}\,, \tag{1b}$$

$$\eta' = \eta - \bar{\eta}\,, \tag{1c}$$

$$\boldsymbol{u}' = \boldsymbol{u} - \bar{\boldsymbol{u}}\,, \tag{1d}$$

where $\boldsymbol{u} = (u, v)$ denotes SSV, η is the SSH, $\zeta = \frac{\partial v}{\partial x} - \frac{\partial u}{\partial y}$ the vertical component of the relative vorticity (hereafter referred to as relative vorticity), Π the linearized potential vorticity anomaly relative to the rest state, g the acceleration due to gravity, $\boldsymbol{f_0} = (0, 0, f_0)$ with f_0 being the Coriolis parameter on the f-plane and L_d the deformation radius. Overbars and primes represent vortical and wavy variables, respectively. Physically, Equation 1a implies that the potential vorticity anomaly, which can be derived from the full flow variables, is entirely due to vortical motions; mathematically, Equation 1a is a Helmholtz equation without involving any temporal information, thus allowing vortical SSH (i.e., $\bar{\eta}$) to be inverted from a snapshot of SSH and SSV. Then vortical SSV (i.e., $\bar{\boldsymbol{u}}$) is derived from vortical SSH based on the geostrophic balance in Equation 1b. Finally, wavy variables (i.e., η' and $\boldsymbol{u}'$) are recovered via Equations 1c-1d as the differences between the full and vortical fields. Therefore, Equations

---

[1] Pedlosky (2003) provides a simpler explanation from the perspective of the potential vorticity conservation. For the wavy motion, the conservation equation is $\partial\Pi'/\partial t=0$, where Π' is the wavy potential vorticity anomaly relative to the rest state. Assuming the periodic wavy motion has a frequency ω, $\partial\Pi'/\partial t=0$ becomes $\omega\Pi'=0$. Since ω is non-zero, Π' must be zero.

1a-1d provide a framework for a snapshot-based decomposition of SSH and SSV into vortical and wavy components.

2.2 Determination of the deformation radius

A crucial step in the abovementioned decomposition is to determine the deformation radius (i.e., L_d) in Equation 1a. In the classic theory, L_d corresponds to only one vertical normal mode (Pedlosky, 2003). This contradicts the real-ocean scenario where the vertical structure is a superposition of many vertical modes, especially when submesoscale processes or high-mode IGWs are active. To practically consider contributions of all vertical modes, Torres et al. (2019) set L_d via requiring that the wavenumber transition from vortical to wavy kinetic energy spectra is continuous; Le Guillou et al. (2021) determined L_d using the four-dimensional variational technique. Here, we propose to determine L_d by fitting the wavy potential vorticity anomaly (i.e., $\Pi' = \frac{\partial v'}{\partial x} - \frac{\partial u'}{\partial y} - \frac{1}{L_d^2} \frac{g\eta'}{f_0}$) to zero, which leads to an effective deformation radius. Of course, wavy SSH and SSV are required *a priori* for the determination of the effective deformation radius. We thus adopt the dynamical decomposition approach devised by C. Wang et al. (2023a), obtaining a baseline of wavy variables to estimate L_d. Their approach takes full advantage of the temporal information of physical variables and is capable of accurately disentangling vortical and wavy motions. Note that optimally constraining the wavy potential vorticity anomaly to zero is equivalent to minimizing the difference between vortical and full potential vorticity anomalies.

To specifically illustrate how this effective deformation radius is determined, we employ the hourly snapshot outputs, ranging from 1 March 2012 to 31 March 2012, of a realistic numerical simulation (i.e., LLC4320). The LLC4320 simulation explicitly includes the full luni-solar tidal potential to partially resolve the internal gravity wave continuum. Details about this simulation can be found in Arbic et al. (2018) and at http://wwwcvs.mitgcm.org/viewvc/MITgcm/MITgcm_contrib/llc_hires/. For comparison, we focus on two oceanic regions indicated by the red and magenta boxes in Fig. 1a, i.e., the central South China Sea (Figs. 1a, 1b) which is characterized by vigorous IGWs but low mesoscale variabilities and the Kuroshio Extension (Figs. 1a, 1c) which has weak IGWs but energetic mesoscale processes. As a first step, we use the dynamical decomposition approach devised by C. Wang et al. (2023a) to obtain baseline wavy SSH and SSV in abovementioned two oceanic regions. Then the spatial mean and trend are removed for each hourly snapshot of baseline wavy SSH and SSV, the reason for which will become clear in Section 2.3. Finally, fitting the

baseline wavy potential vorticity anomaly at each instant to zero in a least-square sense yields the effective deformation radius, whose time series is shown in Fig. 2. In the South China Sea (Fig. 2a) and around the Kuroshio Extension (Fig. 2b), the effective deformation radii vary substantially with time and their temporal averages are both ~34 km. Recall that the first baroclinic deformation radius (i.e., c_1/f_0 where c_1 is the phase speed of the first baroclinic mode of gravity waves. See Pedlosky (2003) for details.) is ~59 km in the South China Sea and ~34 km around the Kuroshio Extension. It would be interesting to figure out the exact cause of the contrast (similarity) between the effective and first deformation radii in the South China Sea (Kuroshio Extension), which is, however, beyond the scope of this study. Hereafter, the temporal averages of the effective deformation radius in each region will be used for convenience.
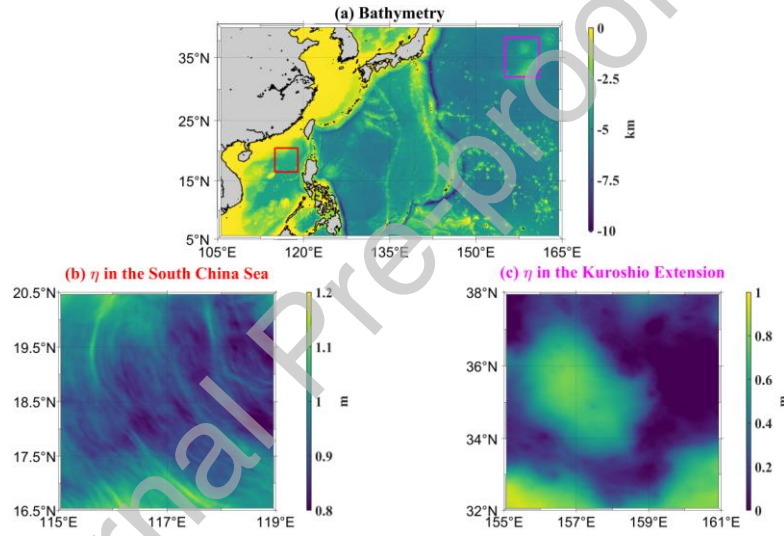

Fig. 1. Bathymetry of the northwestern Pacific (a), an SSH snapshot for the central South China Sea (b) highlighted by the red box, and an SSH snapshot for the subregion around the Kuroshio Extension (c) highlighted by the magenta box.
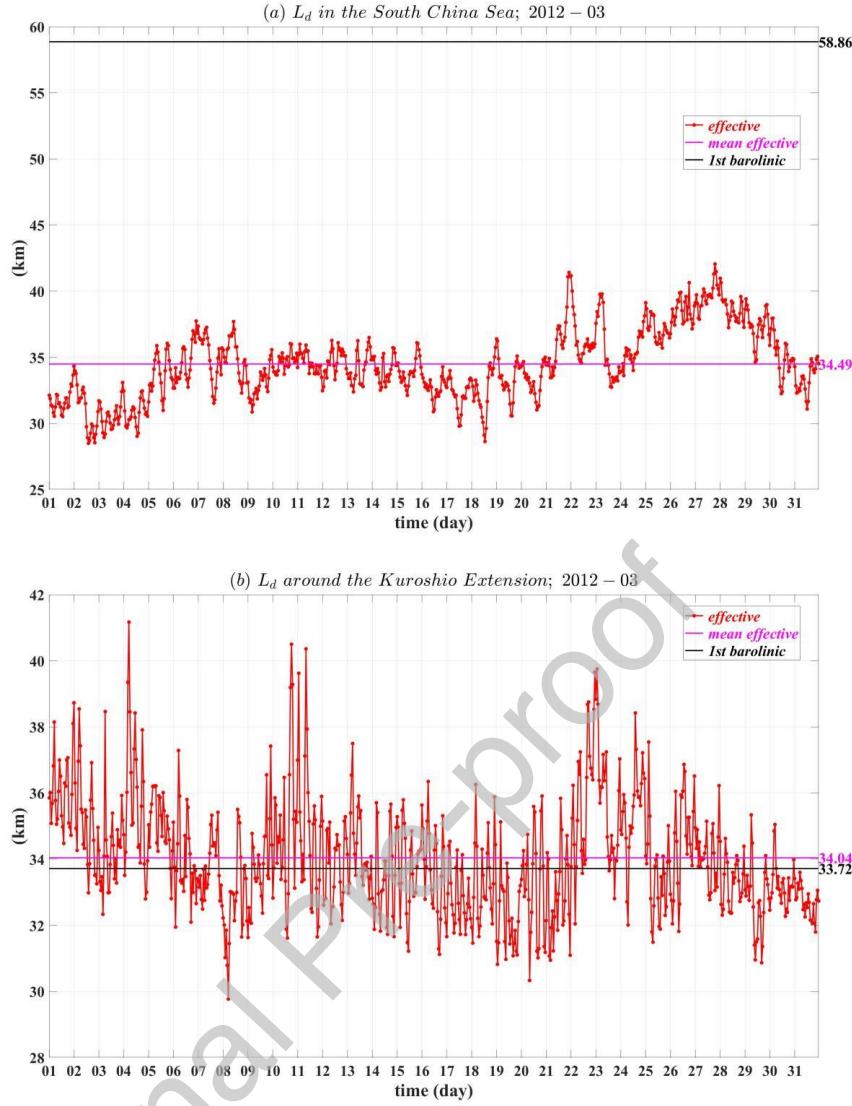
Fig. 2. The deformation radius in the central South China Sea (a) and the subregion around the Kuroshio Extension (b). The red line denotes the hourly time series of the effective deformation radius whose temporal mean is represented by the magenta line. The black line shows the first baroclinic deformation radius averaged in the respective oceanic regions.

2.3 Application procedures

With the deformation radius determined in Section 2.2, we are now ready to apply the proposed snapshot-based decomposition to the LLC4320 simulation in the two oceanic regions. Technically, the Fourier transform is applied to Equation 1a to invert vortical SSH at each instant in time. As is standard, the mean and trend of SSH and SSV are removed and a Tukey window with a taper-constant ratio of 0.2 (Arbic et al., 2014) is imposed before the Fourier transform; therefore, η and $\boldsymbol{u}$ in Equations 1a, 1c, 1d respectively represent detrended-demeaned-windowed SSH and SSV, which necessitates the detrending and demeaning in

9

estimating the deformation radius in Section 2.2. With vortical SSH known, the Fourier transforming of Equation 1b gives vortical SSV. Finally, wavy SSH and SSV are calculated using Equations. 1c-1d, respectively. Note that since large-scale currents and barotropic tides are removed during the process of detrending, demeaning and windowing (C. Wang et al., 2023b), vortical motions from Equations 1a-1d mainly include mesoscale and submesoscale flows and wavy motions generally involves IGWs.

3. Proof-of-concept Application

3.1 Decomposed results

Figure 3 shows the decomposed wavy and vortical SSH (η), zonal velocity (U) and meridional velocity (V) in the South China Sea and around the Kuroshio Extension. In the South China Sea, wavy variables (Figs. 3a-3c) clearly exhibit southwestward-propagating IGWs which are mostly baroclinic tides generated in the Luzon Strait. The wavy pattern is also easily found in the relative vorticity (ζ; Fig. 4a) and horizontal divergence (χ; Fig. 4b), although Figures 4a-4b are dominated by much finer horizontal scales whose contributions are amplified when spatial derivatives are taken to calculate the relative vorticity and horizontal divergence (C. Wang et al., 2023b). Constrained by the wave dynamics, most energies of the wavy motion are distributed at tidal frequencies and along dispersion relation curves of the first and second-mode IGWs as shown by the frequency-wavenumber spectra (Figs. 5a and 5d) which are computed after the decomposition is applied to each snapshot of SSH and SSV. Note that the spectral energies of IGWs in Figs. 5a and 5d fold back into the subinertial band at ~0.1 cpkm after reaching the highest frequency (i.e., 0.5 cph) because IGWs with a frequency higher than 0.5 cph are aliased in the hourly snapshot output of the LLC4320 simulation (C. Wang et al., 2022). This suggests that the proposed decomposition approach can well handle the aliasing problem, and can thus successfully recover the aliased IGWs in the decomposed wavy variables. By contrast, spectral energies of the vortical motion in the South China Sea (Figs. 5b and 5e) are mostly subinertial. Vortical SSH and SSV (Figs. 3d-3f) consistently display mesoscale features that are in geostrophic balance. Also present, especially in the zonal velocity (Fig. 3e), are submesoscale flows which can be more readily identified in Fig. 4c as high-vorticity stripes following the large-scale circulation in the southern part of the domain. By construction (i.e., Equation 1b), the decomposition approach yields vortical motions with exactly zero horizontal divergence (Fig. 4d). As shown in Figs. 5a (5b) and 5d (5e), some vortical (wavy) energies leak into the wavy (vortical) motions. For example, there exist

10

enhanced energies at tidal frequencies in spectral densities for decomposed vortical variables, and evident subinertial energies in spectral densities for wavy variables. Despite this leakage, the ratios of wavy to vortical spectral densities (Figs. 5c and 5f) illustrate that baroclinic tides, non-tidal IGWs of the first, second and higher modes and the aliased IGWs have already been satisfactorily extracted, with ~1/10 wavy energies leaking.

Comparatively, wavy motions in the Kuroshio Extension are dominated by highly incoherent baroclinic tides with irregular spatial patterns (Figs. 3g-3i, 4e-4f) and still well constrained by dispersion relations of IGWs (Figs. 5g, 5j, 5i and 5l). With most IGWs extracted (Figs. 5h and 5k), the decomposed vortical motions (Figs. 3j-3l and 4g-4h) include mesoscale eddies (one of which is highlighted in Figs. 3j-3l by a red box) and submesoscale eddies (one of which is emphasized by a black box). Submesoscale filaments with high vorticity (Fig. 4g) are also seen especially along the large-scale circulation. Overall, the applications in the South China Sea and around the Kuroshio Extension suggest that the decomposition approach works well irrespective of the dynamical regime of interest.
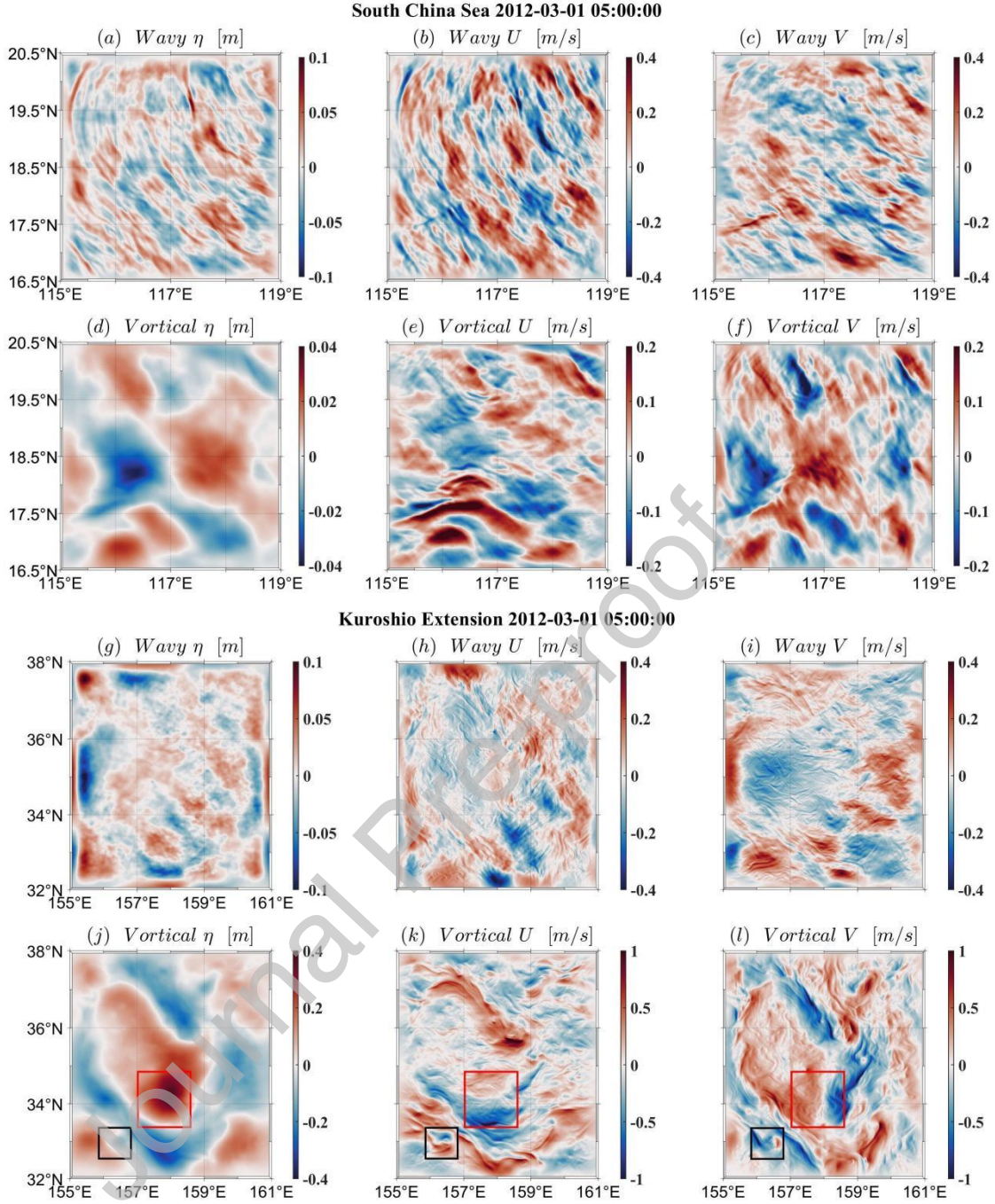
Fig. 3. Example snapshot of the decomposed SSH (η; a, d, g, j), zonal velocity (U; b, e, h, k) and meridional velocity (V; c, f, i, l) associated with wavy (a-c, g-i) and vortical (d-f, j-l) motions in the South China Sea (a-f) and around the Kuroshio Extension (g-l). Red and black boxes in (j, k, l) highlight mesoscale and submesoscale eddies, respectively.
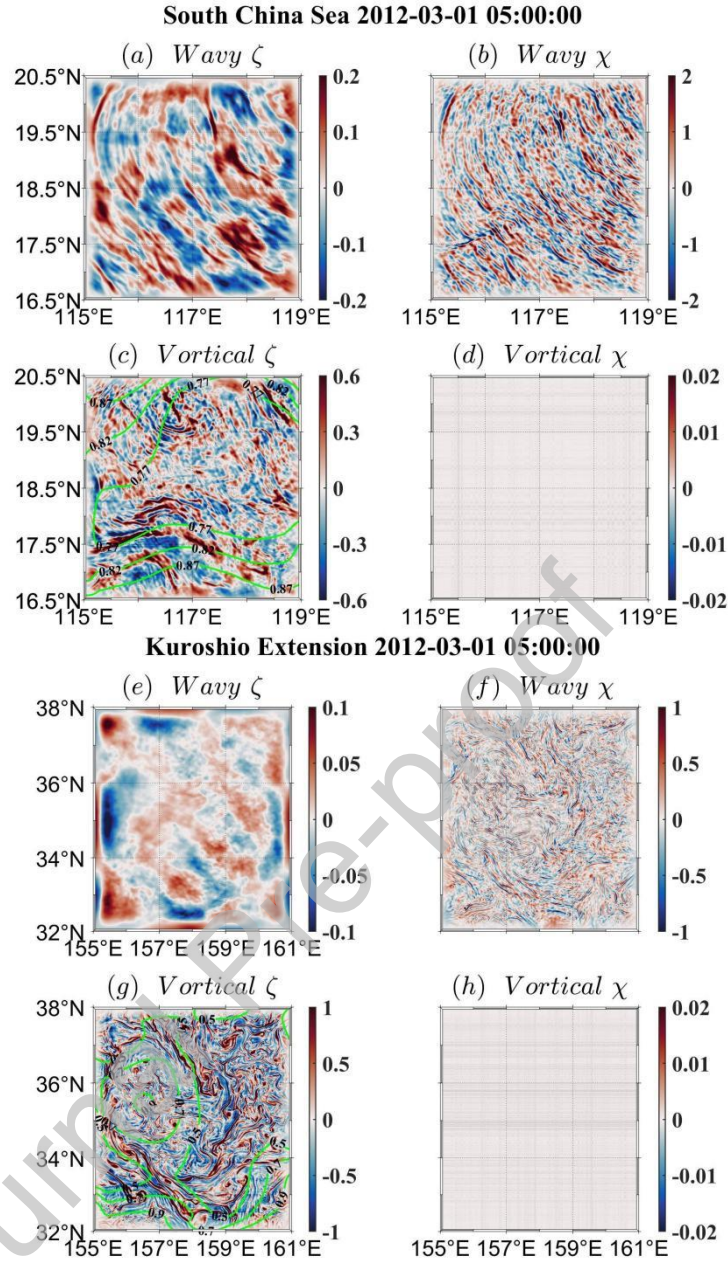
Fig. 4. Example snapshot of the decomposed relative vorticity (ζ; a, c, e, g) and horizontal divergence (χ; b, d, f, h) associated with wavy (a, b, e, f) and vortical (c, d, g, h) motions in the South China Sea (a-d) and around the Kuroshio Extension (e-h). The green contours in (c, g) denote SSH of large-scale currents.
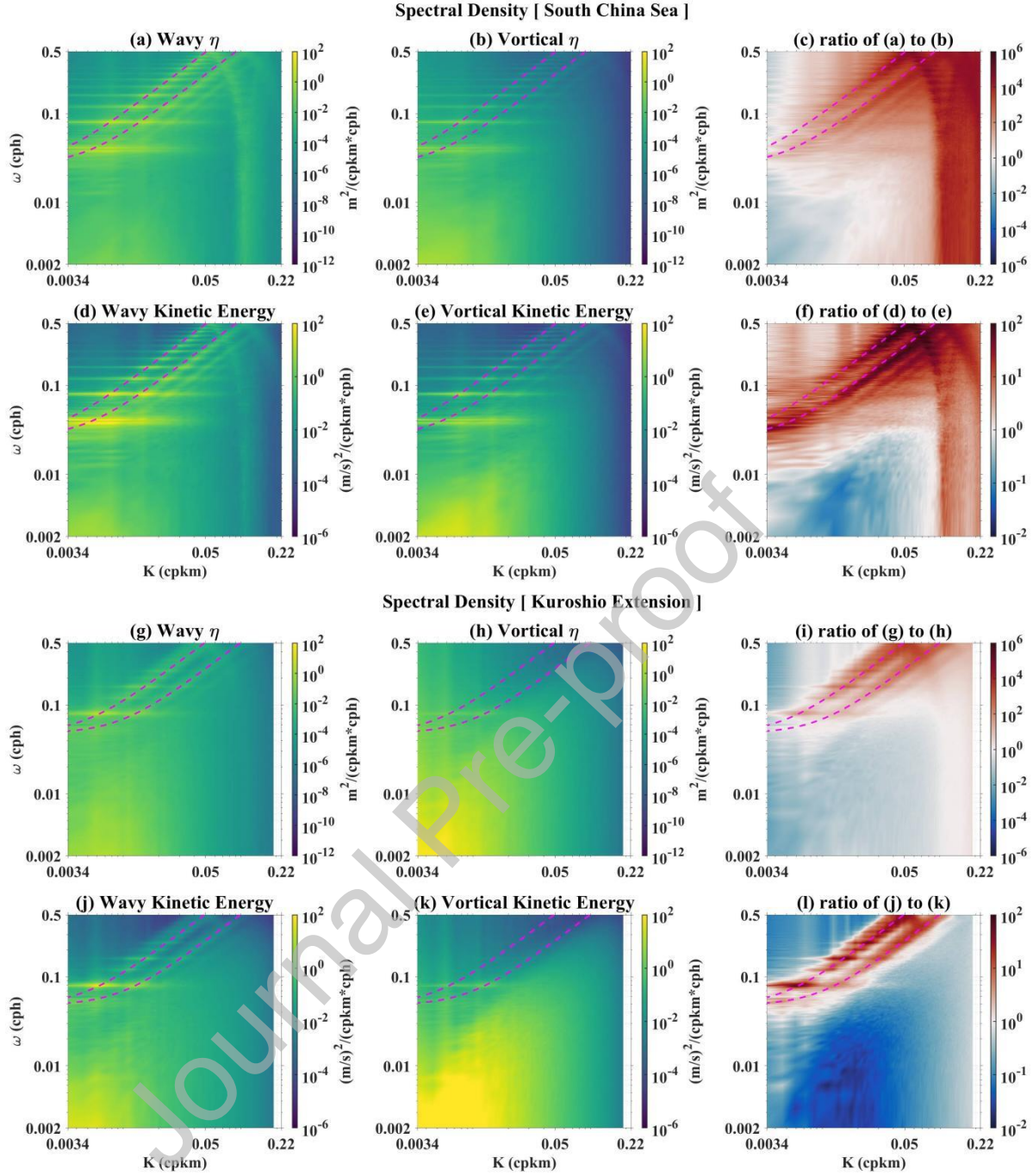
13

Fig. 5. SSH frequency-wavenumber spectra (a, b, g, h) of wavy (a, d, g, j) and vortical (b, e, h, k) motions, horizontal kinetic energy frequency-wavenumber spectra (d, e, j, k) of wavy and vortical motions and spectral density ratios (c, f, i, l) of wavy to vortical motions in the South China Sea (a-f) and around the Kuroshio Extension (g-l). The dashed magenta lines denote dispersion relation curves for IGWs of the first and second baroclinic modes.

3.2 Comparison with the baseline

14

The usefulness of the proposed snapshot-based decomposition approach has been demonstrated in Section 3.1. For further demonstration, this section compares our decomposed results with their baseline counterparts from the dynamical decomposition approach devised by C. Wang et al. (2023a) as mentioned in Section 2.2. Figures 6-8 display a snapshot of the baseline results, together with the root mean square (RMS) errors and correlation coefficients between our snapshot-based decomposed results and baseline results. For wavy motions in the South China Sea, the snapshot-based decomposed results (Figs. 3a-3c) agree well with the dynamically-decomposed baseline results (Figs. 6a-6c) in terms of both the pattern and magnitude. The agreement carries over to the whole study period since the RMS errors of wavy SSH (SSV) are generally smaller than 0.008 m (0.06 m/s) over the entire domain and negligible (Figs. 7a-7c) compared with the typical magnitude of wavy SSH (SSV). Furthermore, the magnitudes of wavy variables given respectively by snapshot-based and dynamical decompositions temporally evolve in a consistent manner as shown by the extremely high correlations, which are above 0.8, over the whole domain except for the edges due to the windowing effect (Figs. 8a-8c). By contrast, RMS errors (correlation coefficients) for vortical motions in the South China Sea are larger (smaller) than those for wavy motions, which is not beyond acceptance though. This is accessible since vortical motions in this region are much weaker than wavy motions as mentioned in Section 2.2 and shown in Figs. 3a-3f and thus any energy leakage of the same magnitude will adversely affect vortical motions more significantly than wavy motions. By contrast, around the Kuroshio Extension, vortical motions are more accurately isolated than wavy motions since vortical motions in this region dominate its wavy counterparts as mentioned in Section 2.1 and shown in Figs. 3g-3l. Otherwise, the proposed decomposition yields consistent results with the baseline results around the Kuroshio Extension. In general, the comparisons with the baseline results in the South China Sea and around the Kuroshio Extension confirm that the proposed snapshot-based decomposition performs well in contrasting dynamical regimes, given that such a decomposition is challenging with only snapshot SSH and SSV available.
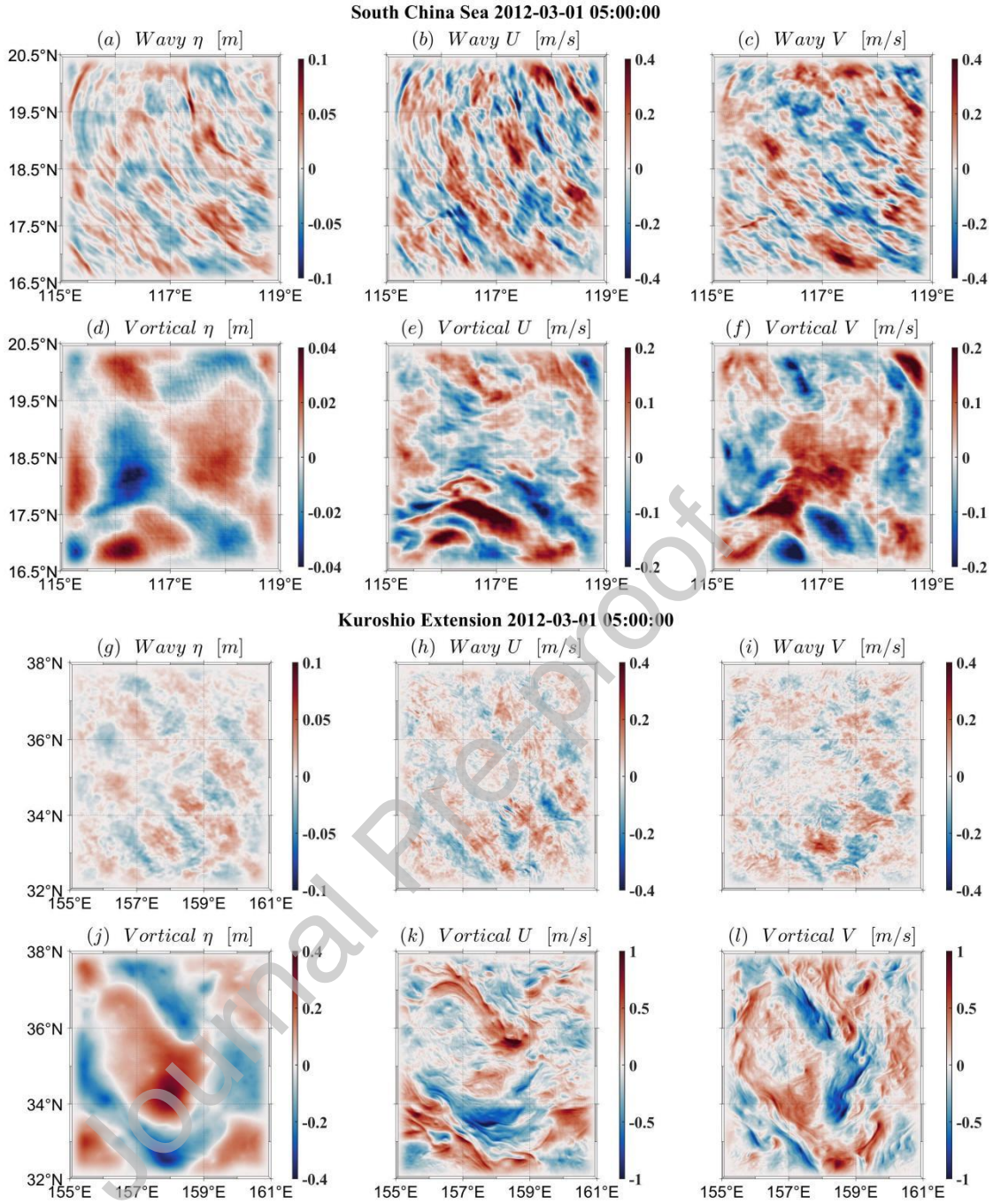
Fig. 6. As in Fig. 3, but for the baseline results. Note that the ranges of colorbars are the same as those of Fig. 3.

Root Mean Square Errors in the South China Sea; 2012-03

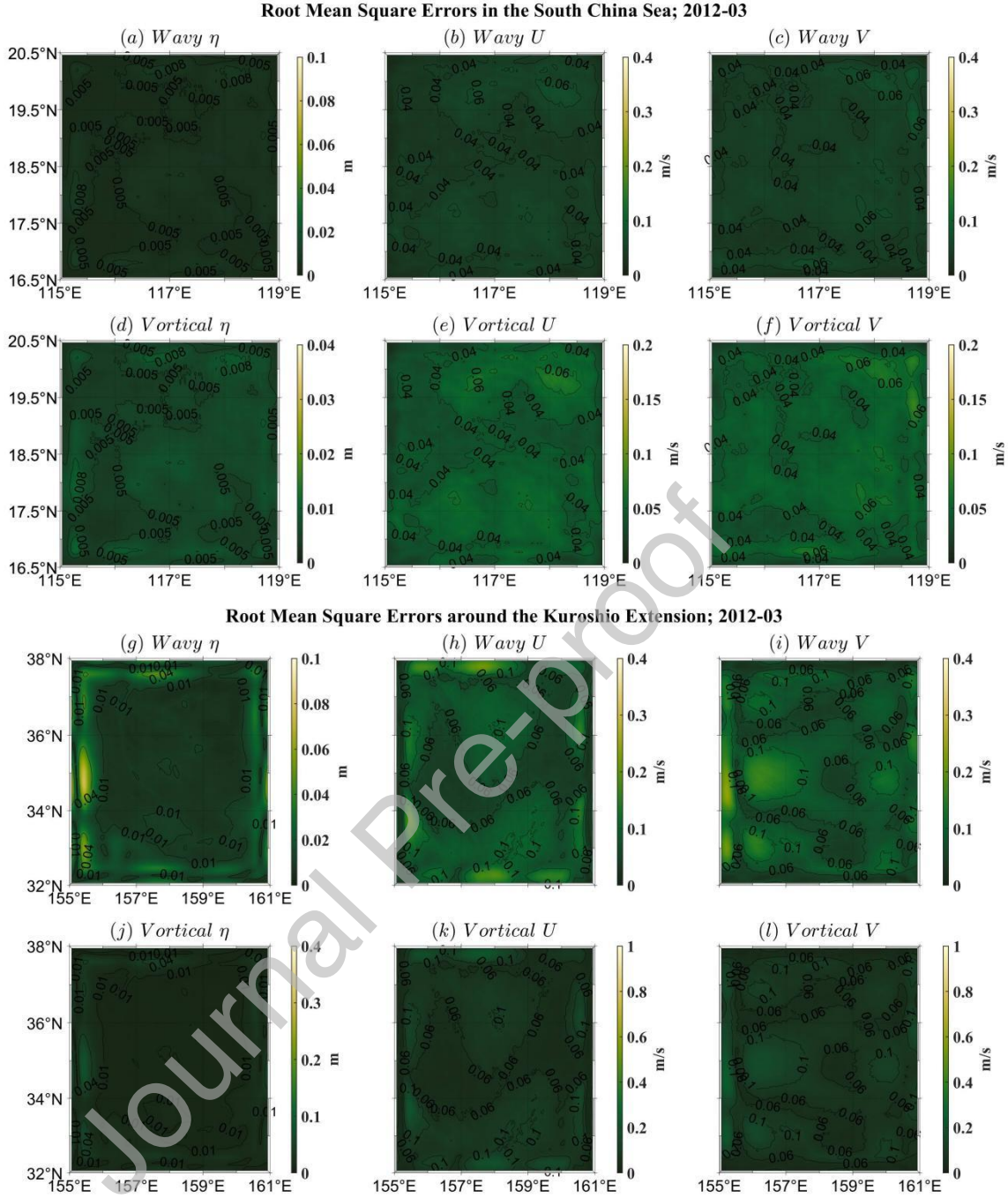Root Mean Square Errors around the Kuroshio Extension; 2012-03

Fig. 7. The root mean square errors between the decomposed wavy variables and their baseline counterparts (a-c, g-i) and root mean square errors between the decomposed vortical variables and their baseline counterparts (d-f, j-l) in the South China Sea (a-f) and around the Kuroshio Extension (g-l). The left (a, d, g and j), middle (b, e, h and k), and right (c, f, i and l) columns show SSH, zonal velocity and meridional velocity, respectively. Note that the ranges of colorbars are the same as those of Figs. 3 and 6.
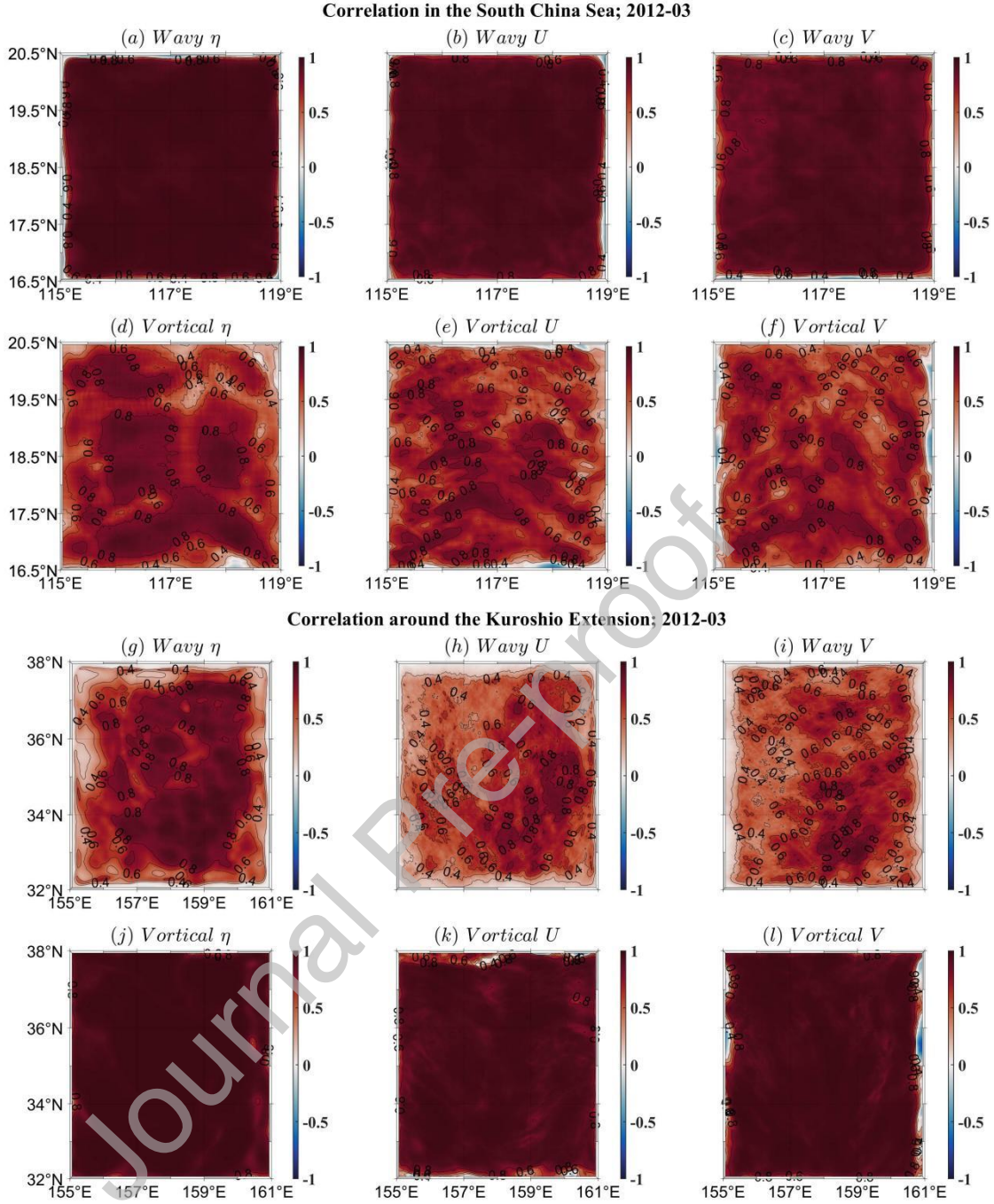
Fig. 8. The pointwise correlation coefficients between the decomposed wavy variables and their baseline counterparts (a-c, g-i) and pointwise correlation coefficients between the decomposed vortical variables and their baseline counterparts (d-f, j-l) in the South China Sea (a-f) and around the Kuroshio Extension (g-l). The left (a, d, g and j), middle (b, e, h and k), and right (c, f, i and l) columns show SSH, zonal velocity and meridional velocity, respectively.

4. Summary and Discussion

Wide-swath satellite missions will concurrently observe SSH and SSV over a two-dimensional region along their tracks but with a long revisit period. It is a formidable challenge to extract various flow components from these observations. This study has shown that the property that wavy motions do not induce any potential vorticity anomaly can be used to develop an approach for decomposing a pair of SSH and SSV snapshots into wavy and vortical components. Proof-of-concept applications to flows from a realistic tide-resolving and submesoscale-admitting simulation have demonstrated that the proposed dynamics-based approach works well in disentangling wavy and vortical motions in contrasting dynamical regimes; satisfactory performances are achieved both in the South China Sea with strong wavy motions but weak vortical motions and around the Kuroshio Extension with strong vortical motions but weak wavy motions. One immediate application of the proposed decomposition approach is to analyze the outputs of high-resolution tide-resolving numerical simulations and develop the parameterization schemes for isopycnal mixing by vortical motions and diapycnal mixing by wavy motions. Another anticipated application involves SSH and SSV measurements in the real ocean. Currently, SSV data from high-frequency radars distributed along the coast and SWOT SSH data are already available and could, in principle, be used for such a decomposition. Such application will probably reveal some interesting coastal phenomena.

While this study represents a useful attempt, several caveats should be noted. First of all, the proposed decomposition is formulated based on the interior quasi-geostrophic theory; thus wind and buoyancy forcing on the ocean surface, which are two main sources/sinks of potential vorticity, are overlooked. Wind forcing basically yields an Ekman flow which is usually of a large scale and already excluded when the detrending is conducted (C. Wang et al., 2023b) as mentioned in Section 2.3. Therefore, wind forcing will not significantly impact our results. The contribution from buoyancy forcing (e.g., diabatic heating) can be described by the surface quasi-geostrophic dynamics. However, the application of the surface quasi-geostrophic theory requires one more surface variable (i.e., sea surface density) in addition to SSH and SSV; furthermore, the surface quasi-geostrophic theory only achieves high efficiency in oceanic regions with intense mesoscale activity, especially during winter (Gonzalez-Haro and Isern-Fontanet, 2012, 2014). Given that the ultimate goal is to only utilize SSH and SSV to achieve a general decomposition, the quantification of the contribution from buoyancy forcing is beyond the scope of this study but deserves future attention.

Second, to propose a practical and useful snapshot-based decomposition, the effective deformation radius is introduced to reduce the three-dimensional PV inversion to a two-dimensional problem. In practice, the effective deformation radius is not known *a priori*. Considering that (i) most of the geostrophic kinetic energy is captured by the barotropic and first baroclinic modes (Wunsch, 1997; Smith and Vallis, 2001) and (ii) the barotropic mode is mostly removed during the detrending (C. Wang et al., 2023b), we have utilized the first baroclinic deformation radius to re-conduct the disentanglement. It is found that vortical and wavy motions are still satisfactorily separated (see Fig. S1 in Supplementary Material); in particular, submesoscale eddies are again correctly attributed to vortical motions (see Fig. S2 in Supplementary Material). It is thus suggested that the first baroclinic deformation radius is used instead whenever the effective one is not available. In addition, we would like to emphasize that the reduction to a two-dimensional PV inversion is probably the main reason for the energy leakage mentioned in Section 3. If instantaneous three-dimensional fields of pressure and horizontal velocities were available, the reduction would be unnecessary, and a more accurate decomposition would be anticipated. In fact, an intelligent unmanned observing system is being developed to measure the three-dimensional ocean at a swift rate (Dong et al., 2023). A three-dimensional view of the ocean is on the horizon.

Last, although it correctly attributes submesoscale flows to vortical motions, the main drawback of the proposed decomposition is to assume that all vortical motions are in geostrophic balance, which may become invalid for high-frequency submesoscale motions. To address this drawback, more advanced initialization techniques that do not involve any geostrophy-like assumption *a priori*, such as the nonlinear normal mode initialization (Baer and Tribbia, 1977; Machenhauer, 1977), digital filter initialization (Lynch et al., 1997; Lynch and Huang, 1992), optimal potential vorticity balance (Viúdez and Dritschel, 2004), optimal balance (Masur annd Oliver, 2020), can be invoked instead.

Data Availability Statement

The LLC4320 simulation output can be downloaded from https://data.nas.nasa.gov/ecco/data.php?dir=/eccodata/llc_4320. The code to conduct the snapshot-based decomposition developed in this study is available at https://doi.org/10.5281/zenodo.11392014.

CRediT authorship contribution statement

Chuanyin Wang: Writing – original draft, Investigation, Formal analysis, Conceptualization, Funding acquisition. **Zhiyu Liu**: Writing – review & editing, Investigation, Formal analysis, Conceptualization, Supervision, Funding acquisition. **Hongyang Lin**: Writing – review & editing, Investigation, Formal analysis. **Cesar Rocha**: Writing – review & editing. **Qinghua Yang**: Writing – review & editing, Funding acquisition. **Dake Chen**: Writing – review & editing. **Junbin Gong**: Writing – review & editing.

Declaration of competing interest

The authors declare that they have no conflicts of interest in this work

References

Abdalla, S., Abdeh Kolahchi, A., Ablain, M., Adusumilli, S., Aich Bhowmick, S., Alou-Font, E., et al. (2021). Altimetry for the future: Building on 25 years of progress. *Advances in Space Research*, *68*(2), 319–363. https://doi.org/10.1016/j.asr.2021.01.022

Arbic, B. K., Müller, M., Richman, J. G., Shriver, J. F., Morten, A. J., Scott, R. B., et al. (2014). Geostrophic Turbulence in the Frequency–Wavenumber Domain: Eddy-Driven Low-Frequency Variability*. *Journal of Physical Oceanography*, *44*(8), 2050–2069. https://doi.org/10.1175/jpo-d-13-054.1

Arbic, B. K., Alford, M. H., Ansong, J. K., Buijsman, M. C., Ciotti, R. B., Farrar, J. T., et al. (2018). A Primer on Global Internal Tide and Internal Gravity Wave Continuum Modeling in HYCOM and MITgcm. In *New Frontiers in Operational Oceanography* (pp. 307–392). GODAE OceanView. https://doi.org/10.17125/gov2018.ch13

Baer, F., & Tribbia, J. J. (1977). On Complete Filtering of Gravity Modes Through Nonlinear Initialization. *Monthly Weather Review*, *105*(12), 1536–1539. https://doi.org/10.1175/1520-0493(1977)105<1536:OCFOGM>2.0.CO;2

Bourassa, M. A., Rodriguez, E., & Chelton, D. (2016). Winds and currents mission: Ability to observe mesoscale AIR/SEA coupling. In *2016 IEEE International Geoscience and Remote Sensing Symposium (IGARSS)* (Vol. 2016-Novem, pp. 7392–7395). IEEE. https://doi.org/10.1109/IGARSS.2016.7730928

Carrère, L., Le Provost, C., & Lyard, F. (2004). On the statistical stability of the M2 barotropic and baroclinic tidal characteristics from along-track TOPEX/Poseidon satellite altimetry analysis. *Journal of Geophysical Research: Oceans*, *109*(3), 1–13. https://doi.org/10.1029/2003jc001873

Chen, G., Tang, J., Zhao, C., Wu, S., Yu, F., Ma, C., et al. (2019). Concept design of the "Guanlan" science mission: China's novel contribution to space oceanography. *Frontiers in Marine Science*, *6*(MAR), 1–14. https://doi.org/10.3389/fmars.2019.00194

Dong, C., Chen, D., Wang, D., Xu, W., Lian, T., Dai, S., et al. (2023). Intelligent Swift Ocean Observing System. *Ocean-Land-Atmosphere Research*, *2*, 6–8. https://doi.org/10.34133/olar.0022

Dritschel, D. G., & Viúdez, Á. (2007). The persistence of balance in geophysical flows. *Journal of Fluid Mechanics*, *570*(May), 365–383. https://doi.org/10.1017/S0022112006002990

Du, Y., Dong, X., Jiang, X., Zhang, Y., Zhu, D., Sun, Q., et al. (2021). Ocean surface current multiscale observation mission (OSCOM): Simultaneous measurement of ocean surface current, vector wind, and temperature. *Progress in Oceanography*, *193*(January), 102531. https://doi.org/10.1016/j.pocean.2021.102531

Dushaw, B. D. (2015). *An Empirical Model for Mode-1 Internal Tides Derived from Satellite Altimetry : Computing Accurate Tidal Predictions at Arbitrary Points over the World Oceans*. https://doi.org/http://www.apl.washington.edu/project/%0Aprojects/tm_1-15/pdfs/tm_1_15.pdf

Egbert, G. D., & Ray, R. D. (2000). Significant dissipation of tidal energy in the deep ocean inferred from satellite altimeter data. *Nature*, *405*(6788), 775–778. https://doi.org/10.1038/35015531

Egbert, Gary D., & Ray, R. D. (2001). Estimates of M2 tidal energy dissipation from TOPEX/Poseidon altimeter data. *Journal of Geophysical Research: Oceans*, *106*(C10), 22475–22502. https://doi.org/10.1029/2000jc000699

Egbert, Gary D., & Ray, R. D. (2003). Semi-diurnal and diurnal tidal dissipation from TOPEX/Poseidon altimetry. *Geophysical Research Letters*, *30*(17), 1–4. https://doi.org/10.1029/2003gl017676

Fu, L.-L., & Chelton, D. B. (2001). Chapter 2 Large-Scale Ocean Circulation. In *International Geophysics* (Vol. 69, pp. 133–viii). https://doi.org/10.1016/S0074-6142(01)80147-9

Fu, L., Pavelsky, T., Cretaux, J., Morrow, R., Farrar, J. T., Vaze, P., et al. (2024). The Surface Water and Ocean Topography Mission: A Breakthrough in Radar Remote Sensing of the Ocean and Land Surface Water. *Geophysical Research Letters*, *51*(4), 1–9. https://doi.org/10.1029/2023GL107652

Fu, L. L., & Ubelmann, C. (2014). On the transition from profile altimeter to swath altimeter for observing global ocean surface topography. *Journal of Atmospheric and Oceanic Technology*, *31*(2), 560–568. https://doi.org/10.1175/JTECH-D-13-00109.1

Gent, P. R., & Mcwilliams, J. C. (1990). Isopycnal Mixing in Ocean Circulation Models. *Journal of Physical Oceanography*, *20*(1), 150–155. https://doi.org/10.1175/1520-0485(1990)020<0150:imiocm>2.0.co;2

Gonzalez-Haro, C., & Isern-Fontanet, J. (2012). Ocean surface currents reconstruction at a global scale from microwave measurements. *International Geoscience and Remote Sensing Symposium (IGARSS)*, 3780–3783. https://doi.org/10.1109/IGARSS.2012.6350494

González-Haro, C., & Isern-Fontanet, J. (2014). Global ocean current reconstruction from altimetric and microwave SST measurements. *Journal of Geophysical Research: Oceans*, *119*(6), 3378–3391. https://doi.org/10.1002/2013JC009728

Gregg, M. C. (2021). *Ocean mixing*. Cambridge University Press.

Griffies, S. M. (1998). The Gent–McWilliams Skew Flux. *Journal of Physical Oceanography*, *28*(5), 831–841. https://doi.org/10.1175/1520-0485(1998)028<0831:TGMSF>2.0.CO;2

Le Guillou, F., Lahaye, N., Ubelmann, C., Metref, S., Cosme, E., Ponte, A., et al. (2021). Joint Estimation of Balanced Motions and Internal Tides From Future Wide-Swath Altimetry. *Journal of Advances in Modeling Earth Systems*, *13*(12), 1–17. https://doi.org/10.1029/2021MS002613

Jayne, S. R. (2009). The Impact of Abyssal Mixing Parameterizations in an Ocean General Circulation Model. *Journal of Physical Oceanography*, *39*(7), 1756–1775. https://doi.org/10.1175/2009JPO4085.1

Kantha, L. H., & Tierney, C. C. (1997). Global baroclinic tides. *Progress in Oceanography*, *40*(1–4), 163–178. https://doi.org/10.1016/S0079-6611(97)00028-1

St. Laurent, L. C., Simmons, H. L., & Jayne, S. R. (2002). Estimating tidally driven mixing in the deep ocean. *Geophysical Research Letters*, *29*(23), 19–22. https://doi.org/10.1029/2002GL015633

Lguensat, R., Fablet, R., le Sommer, J., Metref, S., Cosme, E., Ouenniche, K., et al. (2020). Filtering Internal Tides from Wide-Swath Altimeter Data Using Convolutional Neural Networks. In *IGARSS 2020 - 2020 IEEE International Geoscience and Remote Sensing Symposium* (pp. 3904–3907). IEEE. https://doi.org/10.1109/IGARSS39084.2020.9323531

Lynch, P., & Huang, X.-Y. (1992). Initialization of the HIRLAM Model Using a Digital Filter. *Monthly Weather Review*, *120*(6), 1019–1034. https://doi.org/10.1175/1520-0493(1992)120<1019:IOTHMU>2.0.CO;2

Lynch, P., Giard, D., & Ivanovici, V. (1997). Improving the Efficiency of a Digital Filtering Scheme for Diabatic Initialization. *Monthly Weather Review*, *125*(8), 1976–1982. https://doi.org/10.1175/1520-0493(1997)125<1976:ITEOAD>2.0.CO;2

Machenhauer, B. (1977). On the dynamics of gravity oscillations in a shallow water model, with application to normal mode initialization. *Beitr. Phys. Atmos.*, *50*(December), 253–271.

Masur, G. T., & Oliver, M. (2020). Optimal balance for rotating shallow water in primitive variables. *Geophysical and Astrophysical Fluid Dynamics*, *114*(4–5), 429–452. https://doi.org/10.1080/03091929.2020.1745789

Morrow, R., Fu, L. L., Ardhuin, F., Benkiran, M., Chapron, B., Cosme, E., et al. (2019). Global observations of fine-scale ocean surface topography with the Surface Water and Ocean Topography (SWOT) Mission. *Frontiers in Marine Science*, *6*(APR), 1–19. https://doi.org/10.3389/fmars.2019.00232

Morrow, R., Fu, L.-L., Rio, M.-H., Ray, R., Prandi, P., Le Traon, P.-Y., & Benveniste, J. (2023). Ocean Circulation from Space. *Surveys in Geophysics*, (0123456789). https://doi.org/10.1007/s10712-023-09778-9

Pedlosky, J. (2003). *Waves in the Ocean and Atmosphere*. Berlin, Heidelberg: Springer Berlin Heidelberg. https://doi.org/10.1007/978-3-662-05131-3

Ponte, A. L., Klein, P., Dunphy, M., & Le Gentil, S. (2017). Low-mode internal tides and balanced dynamics disentanglement in altimetric observations: Synergy with surface density observations. *Journal of Geophysical Research: Oceans*, *122*(3), 2143–2155. https://doi.org/10.1002/2016JC012214

Provost, C. (2001). Chapter 6 Ocean Tides. *International Geophysics*, *69*, 267–303. https://doi.org/10.1016/S0074-6142(01)80151-0

Ray, R. D., & Zaron, E. D. (2016). M2 internal tides and their observed wavenumber spectra from satellite altimetry. *Journal of Physical Oceanography*, *46*(1), 3–22. https://doi.org/10.1175/JPO-D-15-0065.1

Ray, Richard D., & Cartwright, D. E. (2001). Estimates of internal tide energy fluxes from topex/poseidon altimetry: Central North Pacific. *Geophysical Research Letters*, *28*(7), 1259–1262. https://doi.org/10.1029/2000GL012447

Ray, Richard D., & Mitchum, G. T. (1996). Surface manifestation of internal tides generated near Hawaii. *Geophysical Research Letters*, *23*(16), 2101–2104. https://doi.org/10.1029/96GL02050

Rodríguez, E., Bourassa, M., Chelton, D., Thomas Farrar, J., Long, D., Perkovic-Martin, D., & Samelson, R. (2019). The winds and currents mission concept. *Frontiers in Marine Science*, *6*(JUL), 1–8. https://doi.org/10.3389/fmars.2019.00438

Smith, K. S., & Vallis, G. K. (2001). The Scales and Equilibration of Midocean Eddies: Freely Evolving Flow. *Journal of Physical Oceanography*, *31*(2), 554–571. https://doi.org/10.1175/1520-0485(2001)031<0554:TSAEOM>2.0.CO;2

Torres, H., Wineteer, A., Klein, P., Lee, T., Wang, J., Rodriguez, E., et al. (2023). Anticipated Capabilities of the ODYSEA Wind and Current Mission Concept to Estimate Wind Work at the Air–Sea Interface. *Remote Sensing*, *15*(13), 3337. https://doi.org/10.3390/rs15133337

Torres, H. S., Klein, P., Siegelman, L., Qiu, B., Chen, S., Ubelmann, C., et al. (2019). Diagnosing Ocean-Wave-Turbulence Interactions From Space. *Geophysical Research Letters*, *46*(15), 8933–8942. https://doi.org/10.1029/2019GL083675

Le Traon, P. Y. (2013). From satellite altimetry to Argo and operational oceanography: three revolutions in oceanography. *Ocean Science*, *9*(5), 901–915. https://doi.org/10.5194/os-9-901-2013

Le Traon, P. Y., & Morrow, R. (2001). Chapter 3 Ocean Currents and Eddies. In *International Geophysics* (Vol. 69, pp. 171–xi). https://doi.org/10.1016/S0074-6142(01)80148-0

Viúdez, Á., & Dritschel, D. G. (2004). Optimal potential vorticity balance of geophysical flows. *Journal of Fluid Mechanics*, *521*, 343–352. https://doi.org/10.1017/S0022112004002058

Wang, C., Liu, Z., & Lin, H. (2022). Interpreting consequences of inadequate sampling of oceanic motions. *Limnology and Oceanography Letters*, *7*(5), 385–391. https://doi.org/10.1002/lol2.10260

Wang, C., Liu, Z., & Lin, H. (2023a). A Simple Approach for Disentangling Vortical and Wavy Motions of Oceanic Flows. *Journal of Physical Oceanography*, *53*(5), 1237–1249. https://doi.org/10.1175/JPO-D-22-0148.1

Wang, C., Liu, Z., & Lin, H. (2023b). On Dynamical Decomposition of Multiscale Oceanic Motions. *Journal of Advances in Modeling Earth Systems*, *15*(3). https://doi.org/10.1029/2022MS003556

Wang, H., Grisouard, N., Salehipour, H., Nuz, A., Poon, M., & Ponte, A. L. (2022). A Deep Learning Approach to Extract Internal Tides Scattered by Geostrophic Turbulence. *Geophysical Research Letters*, *49*(11), 1–9. https://doi.org/10.1029/2022GL099400

Wunsch, C. (1997). The Vertical Partition of Oceanic Horizontal Kinetic Energy. *Journal of Physical Oceanography*, *27*(8), 1770–1794. https://doi.org/10.1175/1520-0485(1997)027<1770:TVPOOH>2.0.CO;2

Zaron, E. D. (2019). Baroclinic tidal sea level from exact-repeat mission altimetry. *Journal of Physical Oceanography*, *49*(1), 193–210. https://doi.org/10.1175/JPO-D-18-0127.1

Zaron, E. D., Musgrave, R. C., & Egbert, G. D. (2022). Baroclinic Tidal Energetics Inferred from Satellite Altimetry. *Journal of Physical Oceanography*, *52*(5), 1015–1032. https://doi.org/10.1175/JPO-D-21-0096.1

Zeitlin, V. (2018). *Geophysical fluid dynamics: understanding (almost) everything with rotating shallow water models*. Oxford University Press.

Zhao, Z. (2017). The Global Mode-1 S2 Internal Tide. *Journal of Geophysical Research: Oceans*, *122*(11), 8794–8812. https://doi.org/10.1002/2017JC013112

Zhao, Z., Alford, M. H., Girton, J. B., Rainville, L., & Simmons, H. L. (2016). Global observations of open-ocean mode-1 M2 internal tides. *Journal of Physical Oceanography*, *46*(6), 1657–1684. https://doi.org/10.1175/JPO-D-15-0105.1

Declaration of interests

☒ The authors declare that they have no known competing financial interests or personal relationships that could have appeared to influence the work reported in this paper.

☐ The authors declare the following financial interests/personal relationships which may be

considered as potential competing interests: